Tissue Engineering

DOI: 10.1089/ten.TEC.2023.0345

Title: Novel sheep model to assess critical-sized bone regeneration with periosteum for in-vivo bioreactors

Authors:

Yohaann A. Ghosh[1,2,3], Hai Xin[1,2], D S Abdullah Al Maruf[1,2], Kai Cheng[1,4], Innes Wise[5], Chris Burrows[5], Ruta Gupta[6], Veronica Ka-Yan Cheung[6], James Wykes[1,2], David Leinkram[1], Catriona Froggatt[1], Will Lewin[7,8,9], Hedi V. Kruse[7,9,10], Eva Tomaskovic-Crook[7,8,10], David R. McKenzie[7,9,10], Jeremy Crook[7,8,9,10], Jonathan R. Clark[1,2,4]

Affiliations:

1. Department of Head & Neck Surgery, Chris O'Brien Lifehouse, Camperdown, 2050, NSW, Australia
2. Sydney Medical School, The University of Sydney, Camperdown, 2050, NSW, Australia
3. School of Medicine & Dentistry, Griffith University, Gold Coast, 4215, QLD, Australia
4. Royal Prince Alfred Institute of Academic Surgery, Sydney Local Health District, NSW, 2050, Australia
5. Laboratory Animal Services, The University of Sydney, Camperdown, 2050, NSW, Australia
6. Department of Tissue Pathology and Diagnostic Oncology, Royal Prince Alfred Hospital, Camperdown, 2050, NSW, Australia
7. Arto Hardy Family Biomedical Innovation Hub, Chris O'Brien Lifehouse, Camperdown, NSW 2050, Australia
8. School of Medical Sciences, Faculty of Medicine and Health, The University of Sydney, NSW, 2050, Australia
9. Sarcoma and Surgical Research Centre, Chris O'Brien Lifehouse, Camperdown, 2050, Australia
10. School of Physics, Faculty of Science, The University of Sydney, Camperdown, 2050, Australia

Corresponding author:

Yohaann A. Ghosh (https://orcid.org/0000-0003-0289-731X)

Email: yohaann.ghosh@lh.org.au

Phone: +61 432209458

1. Department of Head & Neck Surgery, Chris O'Brien Lifehouse, Camperdown, 2050, NSW, Australia
2. Sydney Medical School, The University of Sydney, Camperdown, 2050, NSW, Australia
3. School of Medicine & Dentistry, Griffith University, Gold Coast, 4215, QLD, Australia

Running head (60 Characters Limit): Novel periosteum flaps in sheep to assess bone regeneration.

Key words: Bone; Periosteum; Maxillofacial regeneration; Sheep model; Bioreactor

Author Contact Information and Mailing Address:

Yohaann A. Ghosh:

Department of Head & Neck Surgery, 119-143 Missenden Rd, Camperdown NSW 2050 Australia

yohaann.ghosh@lh.org.au

+61432209458

Hai Xin:

Department of Head & Neck Surgery, 119-143 Missenden Rd, Camperdown NSW 2050 Australia

hai.xin@sydney.edu.au

(02) 8514 0000

D S Abdullah Al Maruf:

Department of Head & Neck Surgery, 119-143 Missenden Rd, Camperdown NSW 2050 Australia

maruf.almaruf@lh.org.au

(02) 8514 0000

Kai Cheng:

Department of Head & Neck Surgery, 119-143 Missenden Rd, Camperdown NSW 2050 Australia

kai.cheng@health.nsw.gov.au

(02) 8514 0000

Innes Wise:

Laboratory Animal Services, John Hopkins Dr, Camperdown NSW 2050 Australia

innes.wise@sydney.edu.au

(02) 8627 1616

Chris Burrows:

Laboratory Animal Services, John Hopkins Dr, Camperdown NSW 2050 Australia

chris.burrows@sydney.edu.au

(02) 8627 1616

Ruta Gupta:

Department of Tissue Pathology and Diagnostic Oncology, Bld 94, Royal Prince Alfred Hospital, John Hopkins drive, Camperdown NSW 2050 Australia

ruta.gupta@health.nsw.gov.au

02 9515 8353

Tissue Engineering
Novel sheep model to assess critical-sized bone regeneration with periosteum for in-vivo bioreactors (DOI: 10.1089/ten.TEC.2023.0345)
This paper has been peer-reviewed and accepted for publication, but has yet to undergo copyediting and proof correction. The final published version may differ from this proof.

Veronica Ka-Yan Cheung:

Department of Tissue Pathology and Diagnostic Oncology, Bld 94, Royal Prince Alfred Hospital, John Hopkins drive, Camperdown NSW 2050 Australia

veronica.cheung@health.nsw.gov.au

02 9515 8353

James Wykes:

Department of Head & Neck Surgery, 119-143 Missenden Rd, Camperdown NSW 2050 Australia

james.wykes@lh.org.au

(02) 8514 0000

David Leinkram:

Department of Head & Neck Surgery, 119-143 Missenden Rd, Camperdown NSW 2050 Australia

dl@esoms.com.au

(02) 8514 0000

Catriona Froggatt:

Department of Head & Neck Surgery, 119-143 Missenden Rd, Camperdown NSW 2050 Australia

cate.froggatt@lh.org.au

(02) 8514 0000

Will Lewin:

Arto Hardy Family Biomedical Innovation Hub, 119-143 Missenden Rd, Camperdown NSW 2050 Australia

Tissue Engineering
Novel sheep model to assess critical-sized bone regeneration with periosteum for in-vivo bioreactors (DOI: 10.1089/ten.TEC.2023.0345)

will.lewin@lh.org.au

(02) 8514 0000

Hedi V. Kruse:

Arto Hardy Family Biomedical Innovation Hub, 119-143 Missenden Rd, Camperdown NSW 2050 Australia

hedi.kruse@lh.org.au

(02) 8514 0000

Eva Tomaskovic-Crook:

Arto Hardy Family Biomedical Innovation Hub, 119-143 Missenden Rd, Camperdown NSW 2050 Australia

eva.tomaskoviccrook@lh.org.au

(02) 8514 0000

David R. McKenzie:

Arto Hardy Family Biomedical Innovation Hub, 119-143 Missenden Rd, Camperdown NSW 2050 Australia

david.mckenzie@sydney.edu.au

(02) 8514 0000

Jeremy Crook:

Arto Hardy Family Biomedical Innovation Hub, 119-143 Missenden Rd, Camperdown NSW 2050 Australia

jeremy.crook@lh.org.au

(02) 8514 0000

Tissue Engineering
Novel sheep model to assess critical-sized bone regeneration with periosteum for in-vivo bioreactors (DOI: 10.1089/ten.TEC.2023.0345)

Jonathan R. Clark:

Department of Head & Neck Surgery, 119-143 Missenden Rd, Camperdown NSW 2050 Australia

jonathan.clark@lh.org.au

(02) 8514 0000

Tissue Engineering
Novel sheep model to assess critical-sized bone regeneration with periosteum for in-vivo bioreactors (DOI: 10.1089/ten.TEC.2023.0345)

Abstract

Considerable research is being undertaken to develop novel biomaterials-based approaches for surgical reconstruction of bone defects. This extends to 3D printed materials that provide stable, structural, and functional support in vivo. However, few preclinical models can simulate *in vivo* human biological conditions for clinically relevant testing. Here we describe a novel ovine model that allows evaluation of *in vivo* osteogenesis via contact with bone and/or periosteum interfaced with printed polymer bioreactors loaded with biomaterial bone substitutes.

The infraspinous scapular region of 14 Dorset-cross sheep was exposed. Vascularised periosteum was elevated either attached to the infraspinatus muscle or separately. In both cases, the periosteum was supplied by the periosteal branch of the circumflex scapular vessels. In eight sheep, a 3D printed 4-chambered polyetheretherketone (PEEK) bioreactor was wrapped circumferentially in vascularised periosteum. In six sheep, twelve double-sided 3D printed 2-chambered polyetherketone (PEK) bioreactors were secured to the underlying bone allowing direct contact with the bone on one side and periosteum on the other.

Our model enabled simultaneous testing of up to 24 (12 double-sided) 10 x 10 x 5 mm bioreactors per scapula in the flat contact approach or a single 40 x 10 mm four-chambered bioreactor per scapula using the periosteal wrap. De novo bone growth was evaluated using histological and radiological analysis.

Importantly, the experimental model was well tolerated by the animals and provides a versatile approach for comparing the osteogenic potential of cambium on the bone surface and elevated with periosteum. Furthermore, the periosteal flaps were sufficiently large for encasing bioreactors containing biomaterial bone substitutes for applications such as segmental mandibular reconstruction.

Impact Statement

Adequately powered preclinical testing is needed to determine the capacity of biomaterials to support osseointegration, osteoinduction, and osteoconduction. Our novel sheep model uses advanced 3D printed polymer bioreactors and the inherent osteogenic properties of periosteum to assist *de novo* bone growth *in vivo*. Leveraging the large surface area of the infraspinous region of the scapula, periosteum can be surgically raised and wrapped circumferentially around the printed bioreactors or provide dual contact with periosteum and underlying native bone simultaneously. Finally, the versatile model of osteogenesis allows many bioreactors to be implanted whilst minimising the number of animals required for experimentation.

Introduction

Biomaterials-guided bone regeneration (BGBR) is of increasing interest to surgeons and engineers aiming to heal critical sized skeletal defects. 3D printed materials can provide mechanical strength during defect healing with optimised pore geometries and chemical stimulation of osteogenesis [1]. BGBR is already being used clinically in the reconstruction of small bone defects such as alveolar ridge augmentation in dentistry [2]. However, translation of this technology to critical sized defects i.e., those which cannot naturally heal, has been incumbered by a lack of materials with coincident biocompatibility and mechanical strength, the need for expensive exogenous growth factors, such as recombinant bone morphogenic protein [3,4], and clinically relevant models for evaluation. Nonetheless, BGBR holds great potential as a method to replace autologous bone grafts and osseous free flaps (the current gold standard for large maxillomandibular defects), which can be highly morbid, expensive, and inaccessible to many [5-10].

Material scientists continue to develop novel polymer-, ceramic-, and metal-based implants for bone repair [11-13]. However, before such implants can be translated to patients, they must undergo appropriate pre-clinical testing, including in large animal models. The models should replicate the defect site and native tissue response, ideally without requiring exogenous growth factors [14] or follow up surgery for implant adjustment or removal.

Osteoinduction, osteoconduction, and osseointegration underpin BGBR [15]. Osteoinduction occurs to help bone heal and remodel following injury whereby mesenchymal stem cells are triggered by local chemical and mechanical messengers to promote fracture healing [16]. Further, osteoinduction can be facilitated by periosteum, which harbours a significant bone progenitor cell population [17]. For this reason, periosteal flaps are used clinically to help repair necrotic mandibular bone [18]. However, the osteogenic potential of periosteum can differ between anatomical sites and decreases with age [19]. That is to say, the proliferation and differentiation of osteoblasts is greater in younger animals compared to older ones.

Tissue Engineering
Novel sheep model to assess critical-sized bone regeneration with periosteum for in-vivo bioreactors (DOI: 10.1089/ten.TEC.2023.0345)
This paper has been peer-reviewed and accepted for publication, but has yet to undergo copyediting and proof correction. The final published version may differ from this proof.

In biomaterials science, osteoconduction refers to the complex processes involved with bone formation on the surface of an implant including the proliferation of supporting cells [20,21]. An adequate blood supply is a prerequisite for osteoconduction and depends on the properties of material used, such as structure and surface topology. Investigating this osteoconductive capacity is the focus of much research in biomaterial science and a relevant application for the ovine model presented in this manuscript. Osseointegration refers to the direct contact of living bone on an implant surface for biomechanical anchorage [22]. Histologically, a completely osseointegrated implant will not demonstrate any fibrous tissue growth at the bone-implant interface [20], and is a necessary requirement for maxillomandibular endosteal implants to sustain mechanical loading over many years.

Sheep have similar skeletal anatomy to humans, display comparable bone turnover rates when older, and can be housed easier than most other large animals [23]. While previous ovine models have been used to cover small bone implants using rib periosteum, this is difficult to translate in humans because of the small surface area available [3,24]. More recently, the tibial corticoperiosteal flap has been used with a bone scaffold, but the cortical portion of the flap is not malleable and therefore is less suited to irregular shaped defects encountered in maxillofacial surgery [1]. Here, we describe the use of periosteum from the infraspinous region of the scapula in older sheep for assessing bone substitutes in vivo that are contained within advanced 3D printed polymer bioreactors and without exogenous growth factors. Two novel periosteal flap designs are presented for wrapping or flat-contact with the bioreactors.

Methods

Ethics approval was obtained from The University of Sydney Animal Research Ethics Committee (2020/1817 & 2021/2004).

Cadaveric Study

Three thoracic limbs from skeletally mature dorset-cross sheep (*Ovis aries*) cadavers were examined to define the anatomical boundaries and blood supply to the infraspinous region of the scapula. The sheep scapula has the same bony landmarks as the human scapula as

shown in Figure 1, with the addition of a large cartilaginous border that extends across its length dorsally and caudally. The infraspinatus muscle arises from the infraspinous fossa and scapular spine, inserting onto the greater tubercle of the humerus. The teres major muscle arises from the caudal angle of the scapula and inserts into the greater tubercle of the humerus [25]. Periosteum in this region can be separated from the underlying cortical bone with relative ease in younger sheep but is more challenging when older (Figure 2). It is also more difficult to elevate closer to the glenoid fossa, where it tends to fragment. Blood supply is via branches of the subscapular artery, predominantly through the circumflex scapular artery, which supplies perforating branches to the border of the scapula and muscular branches to teres major and infraspinatus.

Concept development

To utilise the osteogenic properties of periosteum within the bioreactor, two surgical approaches were used. In the first approach (Group A), printed PEEK bioreactors were wrapped circumferentially in vascularised periosteum, with the whole external surface of the bioreactor contents in contact with cambium as shown in Figure 3A. This maximised the surface area of the bioreactor-periosteum interface. However, the second approach (Group B) allowed the model to compare osteogenesis of the PEK bioreactor through contact with periosteum and bone simultaneously. Figure 3D demonstrates how the separation of two chambers arranged in a 'H-shape' accommodates dual contact for simultaneous testing.

Fabrication of Printed PEEK and PEK Bioreactor Scaffolds

PEEK bioreactor scaffolds were fabricated in-house as previously described [26] using an AON M2 (AON3D, Montreal, Canada) fused filament fabrication (FFF) 3D printer. The PEEK material was ThermaXTM PEEK filament (3DXTech, Grand Rapids, Michigan USA, batch 49-122619-06JV). The bioreactors were printed with a 0.4 mm diameter hardened steel nozzle on a polyetherimide build plate with a raft of PEEK to prevent contamination of the bioreactors. The FFF PEEK bioreactor design depicted in Figure 3A was cross shaped in cross-section dividing the 10 x 10 x 40 mm rectangular prism into four chambers, providing space for four separate biomaterial bone substitutes to be housed concurrently. Post-

printing processing involved annealing to complete the crystallization process. Scaffolds were placed in a dry oven with the temperature steadily increased to 200℃ before being held at this temperature for two hours and then steadily returned to room temperature.

PEK bioreactor scaffolds were fabricated in-house using PEEK HP3 powder (EOS GmbH, Krailling, Germany) and an EOS P800 (EOS GmbH, Krailling, Germany) high temperature selective laser sintering (SLS) 3D printer. After printing and cooldown, the scaffoldswere removed from the powder cake of the finished print and blasted free of un-sintered powder with dry ice using a ColdJet Microclean at 1.8 bar gauge pressure and a feed rate of 0.15 kg /min (ColdJet, Loveland, Ohio USA). The SLS PEK bioreactor design in Figure 3D was H shaped in cross-section with two chambers of 10 x 10 x 5 mm, providing separate zones for biological contact.

Experimental animals

Fourteen elderly dorset-cross sheep (12 female, 2 male, age 6-8 years) were obtained from the University of Sydney laboratory animal services and acclimatised to the study facility for at least two weeks. Animals were housed in a minimum of pairs to prevent distress in a temperature controlled indoor facility with straw bedding and fed a diet of wheaten chaff and oaten hay.

Anaesthesia

All animals received a complete physical examination by a specialist veterinarian prior to anaesthesia. Sheep were premedicated intravenously (IV) with a combination of methadone (Troy Animal Care, Glendenning, Australia) 0.2 mg/kg and midazolam 0.4 mg/kg. Anaesthesia was inducted with propofol (Propofol Lipuro, B. Braun, Melsungen, Germany) administered intravenously to facilitate orotracheal intubation. Anaesthesia was maintained with 1-2% inspired isoflurane (Laser Animal Health) delivered in an air/oxygen mixture. Prior to surgery both fetlocks were shaved, and one 50 mcg fentanyl patch (Sandoz, Basel, Switzerland) was applied to each leg (approximately 2 mcg/kg total). Patches were secured using tape and a layer of Vetwrap to prevent dislodgement.

Meloxicam (Troy Animal Care, Glendenning, Australia) 0.5 mg/kg was administered intravenously prior to moving the animal to the operating room.

Ketamine (Randlab, Chipping Norton, Australia) was administered at 20 mcg/kg/min IV throughout the procedure following a loading dose of 0.5 mg/kg. Fluid therapy was provided with Hartmann's solution (Baxter, Deerfield, Illinois) at a rate of 5 ml/kg/hr and morphine (DBL, Dhaka, Bangladesh) was administered at 0.2-0.5 mg/kg IV every four hours or as deemed necessary throughout the procedure. All sheep were mechanically ventilated using volume-controlled ventilation with positive end expiratory pressure of 5 cmH20 to maintain normocapnia. Pulse oximetry, non-invasive blood pressure, capnography, temperature, and electrocardiogram were monitored continuously throughout the procedure and mean arterial pressure was maintained at 70 mmHg or above throughout the entire procedure in all sheep. Active warming was provided to all sheep throughout the procedure using Hot Dog and Cocoon warming systems.

Surgical site access

Animals were placed in sternal recumbency, incision sites shaved, sprayed with 10% povidone-iodine (Betadine, Stamford, Connecticut) and draped. The scapula was palpated, and the borders and spine marked using a sterile pen. A 30 cm curvilinear incision was made by electrocautery along the spine of the scapula. Subcutaneous fat and cutaneous omobrachialis was divided, and the junction between latissimus dorsi and trapezius muscles was incised to gain access to the underlying infraspinatus muscle.

Periosteal wrap model (Group A)

Infraspinatus and teres major muscles were detached from the infraspinous fossa using electrocautery, preserving the vascular supply to the periosteum by leaving a 2 mm cuff of muscle attached to bone and preserving its insertion to the humerus. The periosteal branch of the circumflex scapular artery and vein were identified and isolated at the ventral border of the scapula overlying the insertion of the teres major muscle. A large cutaneous perforator was frequently observed, analogous to the parascapular artery in humans, which could be followed retrograde to identify the circumflex scapular vessels.

Tissue Engineering
Novel sheep model to assess critical-sized bone regeneration with periosteum for in-vivo bioreactors (DOI: 10.1089/ten.TEC.2023.0345)

The periosteum was incised at the cartilaginous portion of the scapular tip and stripped from the entire infraspinous fossa using a periosteal elevator, in the direction of the vascular pedicle. Care was taken not to compromise the vascular pedicle and to include the inner cambium layer with the periosteum. The periosteum was wrapped circumferentially around the cross-shaped PEEK scaffolds leaving access at the distal portion of the flap (Figure 4F).

Four different biomaterials were combined with platelet rich fibrin (PRF) and then inserted into the bioreactor: Morselized autologous bone graft from the scapula, bovine xenograft (Bio-Oss®; Geistlich Pharma AG, Wolhusen, Switzerland), porcine xenograft (ZenGro®; Southern Implants, Irene, South Africa), and Calcium Phosphosilicate (NovaBone® Putty; Novabone, Florida, USA). An open-ended 1 ml syringe was used to pack the graft material inside the chambers, ensuring complete contact with periosteal cambium. The edges of the flap were sutured using 4-0 Prolene (Ethicon Inc., Raritan, New Jersey) in an interrupted fashion, being careful to preserve the vascular pedicle.

Infraspinatus was reattached to the cartilaginous caudal border and bony spine with 1-0 Vicryl suture (Ethicon Inc., Raritan, New Jersey) anchored through drilled holes where required. The bioreactor was placed between the infraspinatus and overlying latissimus dorsi muscle and secured in place with interrupted 2-0 Vicryl suture. Deep closure of the wound was achieved with 3-0 Vicryl suture in an interrupted fashion. A wound soaker catheter was introduced subcutaneously, and skin was closed with continuous 3-0 Monocryl, and knots buried to prevent infection.

Periosteal-bone dual contact model (Group B)

Access to the infraspinatus was the same as Group A. The whole muscle belly was detached from the scapula spine and cartilaginous tip using electrocautery. Then the periosteum was raised using a sharp periosteal elevator with the infraspinatus and teres major muscles together leaving its blood supply via the ventral border and insertion to the humerus intact. Caution was taken not to compromise the vascular pedicle and to include the inner cambium layer with the periosteum and muscle.

After raising the musculoperiosteal flap, each bioreactor was secured to the scapular bone with two 2 x 11 mm titanium screws (KLS Martin, Mühlheim, Germany). The musculoperiosteal flap was then lowered onto the bioreactor, such that the cambium was in contact with the superficial surface (Figure 5F). Infraspinatus was reattached to the cartilaginous caudal border and bony spine with 1-0 Vicryl suture anchored through drilled holes. Deep closure of the wound was achieved with 3-0 Vicryl suture in an interrupted fashion. A wound soaker catheter was introduced subcutaneously, and skin was closed with continuous 3-0 Monocryl.

Three graft materials were used separately for these chambers: bovine xenograft (Bio-Oss®) mixed with PRF, Polycaprolactone-GelatinMethAcryloyl (PCL-GelMA; Translational Research Initiative for Cell Engineering and Printing, Wollongong, Australia), and PCL-GelMA-tricalcium phosphate (PCL-GelMA-TCP; Bionnovation Biomedical, São Paulo, Brazil).

Animal recovery

At the end of the procedure, the wound soaker catheter was loaded with 1 mg/kg of bupivacaine (Pfizer, Tokyo, Japan) diluted 50:50 with 0.9% sodium chloride (Baxter, Deerfield, Illinois) to provide pain relief to the surgical site. Prior to recovery, sheep were weaned from mechanical ventilation and the mouth and oropharynx cleared as required. Animals were recovered in their home pens on a thick layer of straw. Continuous pulse oximetry monitoring as well as assessment of respiratory rate and effort were carried out throughout the recovery period with oxygen supplementation via face mask provided if oxygen saturation (SpO2) fell below 90%. Continuous warming was provided using a Cocoon forced warm air system until sheep reached 39^{o}C or until they were ambulatory. Following extubation, sheep were fitted with custom made jackets which housed an elastomeric pump system. Animals were monitored for food intake as well as ambulation at least twice a day for the remainder of the study period.

Postoperative Analgesia

Prior to leaving the sheep overnight a single dose of methadone 0.2 mg/kg was administered intravenously to continue provision of opioid analgesia until the fentanyl

patches were estimated to have reached therapeutic plasma concentrations approximately 12 hours following application. Local anaesthesia of 0.25% bupivacaine mixed with 300 mcg of buprenorphine (Temgesic, Reckitt, Berkshire, England) was delivered to the operative site via the wound soaker catheter twice daily. Pain was assessed using a combination of the sheep grimace scale as well as general behavioural signs of pain by a specialist veterinary anaesthetist three times a day for the first two days, and then twice daily up to one week following surgery.

Complications

Complications were graded according to the Clavien-Dindo Classification (2004) for surgical complications [27].

Sacrifice

Prior to euthanasia sheep were premedicated as previously described and anaesthesia was induced with propofol until loss of consciousness was achieved. Euthanasia was achieved by using a combination of pentobarbitone and potassium chloride administered IV. At the conclusion of the study (14 weeks) the bioreactors were explanted. A minimum of 5 mm of bone was left attached to the lower bioreactors.

Tissue analysis

The materials were non-destructively imaged using a high-resolution microcomputed tomography (micro-CT) imaging (U-CT, MILabs, The Netherlands) controlled by a MILabs workstation (Intel(R) Xeon(R) CPU E5-2690 V4 @2.60GHz, 128G B RAM, 64-bit Operating System). Samples were scanned using an accurate scan mode with ultra-focus magnification and 20 micron resolution (55 kV tube voltage, 0.19 mA tube current, 75 ms exposure time, and 469 mGY dose estimation whilst being imaged 360° at 0.25 degree per step angle). Scanned image sequence were saved in .tif (Tag Image File) format (1536 x 1944 pixels, 16 Bit depth, uncompressed resolution) and transferred to a post-processing workstation (Intel(R) Core (TM) i5-2400 CPU @ 3.10GHz, 4GB RAM, and 32-bit Operating System) for imaging reconstruction. The scan data of one sample was then reconstructed (total of 180 slices) using MILabs-Rec-10.16 software and exported to an imaging file in an

NII (Neuroimaging Informatics Technology Initiative) format for further segmentation and analysis.

Specimens used for histology were fixed in 10% neutral buffered formalin for at least 7 days. A diamond bone saw (Exakt Technologies Inc, Oklahoma City, Oklahoma) was used to section the bioreactors into 5 mm slices, perpendicular to the long access. They were then transferred into tissue cassettes for acid decalcification overnight before processing using a Leica Peloris Tissue Processor (Leica Biosystems, Melbourne, Australia). The sections were embedded in paraffin on a TES Valida® Paraffin Embedding Centre (Medite GmbH, Wollenweberstr, Germany), sectioned at 4 µm thickness with a Leica RM2235 Rotary Microtome (Leica Biosystems, Melbourne, Australia), and mounted on glass slides for H&E staining with Sakura Tissue-Tek Prisma® Automated Slide Stainer (Sakura Fineteck USA, Inc., CA, USA).

Experiment

Surgery was completed on 8 animals in Group A and 6 animals in Group B. The vascular supply to one Group A bioreactor (sheep 6) was found to be compromised at explantation; based on histological analysis ischaemia was estimated to have occurred at week 6.

Analgesia

All sheep in group A were deemed to need rescue analgesia on the first morning following surgery with moderate lameness being noted prior to administration of additional bupivacaine and buprenorphine. Therefore, the pain relief strategy was modified for group B to replace the twice-daily wound-soaker administration in group A with a continuous local infusion of bupivacaine 0.25% at a rate of 2 ml/hr for 72 hrs post-operatively. Two sheep dislodged their elastomeric pumps and thus received additional loading doses of bupivacaine before recommencing bupivacaine infusions and no further analgesic interventions were required.

Complications

There were two Clavien-Dindo grade IV complications, both unrelated to the surgical method, and the remaining complications were grade I. A suspected haemorrhagic stroke caused one animal (Sheep 1) in Group A to not recover from anaesthesia. This animal had a concurrent cranial procedure performed during the same operation and hence the stroke was deemed unrelated to the scapular surgery. The animal was sacrificed after resuscitation efforts failed. One fatal aspiration also occurred in Group A (sheep 2) following induction of anaesthesia. This was discovered at the completion of the surgical procedure and the animal was sacrificed immediately. Serous discharge drained directly from the surgical incision site of one animal (sheep 3), however this resolved spontaneously without intervention. Two animals in Group B (sheep 11 & 12) had local infections at other surgical sites (mandibular and maxillary implants) unrelated to the procedure described, which resolved with antibiotic therapy before the sacrifice date. One animal was provided probiotic therapy during the experiment in response to soft stools (sheep 13).

Histological Analysis

Histological examination of the bioreactors included evaluation of osteoid and bone formation in addition to cartilage formation, histiocytic and foreign body reaction, chronic inflammation (lymphocytic) and fibrosis. Each histological feature was assessed quantitatively from absent to diffusely present (scale of 0 to 3), as presented elsewhere[28]. In the cross-shaped bioreactor wrapped in periosteum, most osteoid production occurred at the edges of the bioreactor chambers adjacent to the periosteum. Fibrous tissue formed around all graft materials. Endochondral ossification was observed in the Bio-Oss and Zengro chambers. The most substantial woven bone development occurred within chambers containing autologous bone graft (Figure 6A).

In the H-shaped dual-contact bioreactors, new bone formation was observed in both the upper (periosteal contacting) and lower (bone contacting) chambers, but more was observed in the chambers contacting bone. Focal osteoid production was observed at the edge of the bioreactors containing GelMA (Figure 7B) and more substantial osteoid was

observed surrounding the implanted material in the bioreactors containing PCL-GelMA-TCP (Figure 7C).

MicroCT Analysis

Radiological assessment of the graft material was achieved using volumetric analysis and bone mineral density. Across all timepoints the greatest mineral density was seen in Bio-Oss chambers, however histological analysis demonstrated that most of the mineral content was not bone (Figures 6B, 7D, 7E).

Discussion

The present protocol describes a novel approach that allows the use of vascularised periosteum to wrap implanted bioreactors (and other biomaterial constructs) circumferentially and permits concomitant contact of biomaterials with periosteum and cortical bone. The protocol differs from previous approaches in that it allows direct *within-subject* comparison of bone and periosteum contact, and in the ability to wrap large complex scaffolds that would be suitable for BGBR reconstruction of critical sized bone defects such as those seen in segmental mandibulectomy.

Periosteum plays a significant role in bone growth, repair, and nutrient supply. Periosteum covers nearly every bone surface in the body, and is attached to the cortical surface by Sharpey's fibres [29]. Histologically, it can be divided into two layers. Firstly, the superficial layer is comprised of a highly vascularised fibrous portion supplying nutrients to the bone and surrounding muscle, as well as a hypocellular fibroelastic portion [30]. It is this fibroelastic contribution that allows the periosteum to be surgically manipulated in our ovine model around bioreactors of any shape. Secondly, the deep inner cambial layer sits in contact with the bone cortex. The cambium harbours great osteogenic potential due to its high concentration of osteoprogenitor cells imbedded within its collagen matrix along with a rich vascular and neural supply [29] [19].. It is likely that more exuberant bone growth would have been observed by using younger sheep, however, it is these older sheep that more closely replicate the adult human bone biology.

Tissue Engineering
Novel sheep model to assess critical-sized bone regeneration with periosteum for in-vivo bioreactors (DOI: 10.1089/ten.TEC.2023.0345)

Clinically, vascularised periosteal flaps are well described as a surgical approach to optimise local bone healing [31]. Periosteal tissue is ideal for use in combination with a bioreactor, providing osteoinduction without the need for exogenous growth factors[32]. Of note, our group has recently investigated the use of scapular periosteal flaps in humans given the large osteogenic surface area, reliable pedicle and low associated morbidity [33]. We have also investigated the possibility of using an *ex vivo* perfusion bioreactor system to preserve the tissue viability of periosteum[34].

Several animal models have been used to assess bone scaffolds using periosteum as an osteogenic source. The majority utilise periosteum from the rib body as summarised in Table 2, and the most used animals included rats, dogs, pigs and sheep [3,24,35]. However, no previous studies have used the scapula as a donor site in animals. Previous techniques are limited by the small surface area of periosteum available for grafting. This challenge is overcome in our model by using periosteum from the broad infraspinous region of the scapula. Our model allowed for simultaneous testing of up to 24 (12 double-sided) 10 x 10 x 5 mm bioreactor chambers per scapula in the flat contact approach or a single 40 x 10 mm four-chambered bioreactor per scapula using the periosteal wrap. This is readily translatable to humans, with scapular periosteum from the infraspinous region having a mean thickness of 1.2 mm and dimension of 13.7 x 9.3 cm [33].

Although sheep are comparable to humans in both size and physiology, several differences were observed during the surgical procedure and recovery. The absolute size of any scapula will be determined by the age and breed of the animal. In our experiments, Dorset-cross sheep between the ages of 6-8 years were used. This allowed us to harvest a large periosteal flap, however skeletally mature animals inherently have a lower osteogenic capacity compared to growing specimens [17]. In addition to the latissimus dorsi and trapezius muscles that overly the scapula in humans, sheep have an additional superficial muscle, the cutaneous omobrachialis, which runs over the lateral surface of the shoulder and extends to the caudal aspect of the scapula [25]. Differences in the skin and wool layers also make dressing the surgical site in sheep somewhat harder. Due to the production of lanolin, sheep skin is too waxy for traditional adhesive dressings. As such, we

opted to use a spray-on waterproof dressing following primary skin closure (OpSite Spray, Smith + Nephew, Watford, England).

Initially we were concerned about the effect that surgery would have on the mobility of the sheep, however the addition of a wound-soaker catheter provided excellent postoperative analgesia in nearly all the sheep implanted. The use of older sheep comes with increased operative risk, particularly in ruminants, as observed in this protocol where two sheep succumbed to complications including aspiration and stroke. Whilst it is important to maximise the utility of each experimental animal, it is important to carefully consider the effect that concurrent experiments may have on each other. In our experience, two sheep were unable to reach their planned euthanasia date resulting in a considerable waste of resources.

Conclusion

In this methods manuscript we describe a novel model for assessing bone regeneration using periosteum and bone from a safely accessible and large surface area in the scapula. Our reproducible and standardised surgical technique optimises the use of experimental animals allowing simultaneous testing of up to 24 bioreactor chambers per scapula in the flat contact approach or a single four-chambered bioreactor per scapula using the periosteal wrap. Following incubation of the bioreactors, various destructive and non-destructive analytical techniques can be used to determine the quality and quantity of bone formed.

CRediT Author Statement:

Yohaann A. Ghosh: Writing - Original Draft, Investigation. **Hai Xin**: Project administration, Investigation, Formal analysis. **D S Abdullah Al Maruf:** Project administration, Investigation, Formal analysis. **Kai Cheng:** Writing - Review & Editing, Investigation, Data Curation. **Innes Wise:** Investigation, Resources. **Chris Burrows:** Writing - Review & Editing, Investigation, Resources. **Ruta Gupta:** Investigation, Formal analysis. **Veronica Ka-Yan Cheung:** Writing - Review & Editing, Investigation, Formal analysis. **James Wykes:** Writing - Review & Editing, Investigation. **David Leinkram:** Writing - Review & Editing, Investigation.

Catriona Froggatt: Writing - Review & Editing, Investigation. **Will Lewin:** Writing - Review & Editing, Investigation. **Hedi V. Kruse:** Investigation. **Eva Tomaskovic-Crook:** Writing - Review & Editing. **David R. McKenzie:** Writing - Review & Editing, Resources. **Jeremy Crook:** Writing - Review & Editing, Resources. **Jonathan R. Clark:** Conceptualization, Methodology, Writing - Review & Editing, Investigation, Supervision.

Y.A.G, **H.X.** and **D.S.A.A.M.** contributed equally to this manuscript.

Funding:

We would like to acknowledge the following sources of funding supporting this research:

The Cancer Institute New South Wales (CINSW 2020/2081), the National Health and Medical Research Council (NHMRC 2023/GNT2024602), Sydney Local Health District, The Lang Walker Family Foundation, the Australia and New Zealand Head and Neck Cancer Society, the Arto Hardy Family, and the Federal Government of Australia through the Sarcoma and Surgical Research Centre.

The authors have no conflicts of interest to declare.

Acknowledgments

The authors acknowledge the facilities and the scientific and technical assistance at the Hybrid Theatre, Sydney Imaging, a Core Research Facility, University of Sydney.

References

1. Sparks DS, Medeiros Savi F, Saifzadeh S, et al. Bone Regeneration Exploiting Corticoperiosteal Tissue Transfer for Scaffold-Guided Bone Regeneration. Tissue Engineering Part C: Methods 2022;28(5):202-213

2. Carpio L, Loza J, Lynch S, et al. Guided bone regeneration around endosseous implants with anorganic bovine bone mineral. A randomized controlled trial comparing bioabsorbable versus non-resorbable barriers. Journal of periodontology 2000;71(11):1743-1749

3. Tatara AM, Koons GL, Watson E, et al. Biomaterials-aided mandibular reconstruction using in vivo bioreactors. Proceedings of the National Academy of Sciences 2019;116(14):6954-6963

4. Melville JC, Tran HQ, Bhatti AK, et al. Is reconstruction of large mandibular defects using bioengineering materials effective? Journal of Oral and Maxillofacial Surgery 2020;78(4):661. e1-661. e29

5. Clark JR, McCluskey SA, Hall F, et al. Predictors of morbidity following free flap reconstruction for cancer of the head and neck. Head & Neck: Journal for the Sciences and Specialties of the Head and Neck 2007;29(12):1090-1101

6. Mazzola F, Smithers F, Cheng K, et al. Time and cost-analysis of virtual surgical planning for head and neck reconstruction: A matched pair analysis. Oral Oncology 2020;100(104491

7. Petrides GA, Dunn M, Charters E, et al. Health-related quality of life in maxillectomy patients undergoing dentoalveolar rehabilitation. Oral Oncol 2022;126(105757

8. Pogrel MA, Podlesh S, Anthony JP, et al. A comparison of vascularized and nonvascularized bone grafts for reconstruction of mandibular continuity defects. Journal of Oral and Maxillofacial Surgery 1997;55(11):1200-1206

9. Marechek A, AlShare A, Pack S, et al. Nonvascularized Bone Grafts for Reconstruction of Segmental Mandibular Defects: Is Length of Graft a Factor of Success? Journal of Oral and Maxillofacial Surgery 2019;77(12):2557-2566

10. Leinkram D, Wykes J, Palme C, et al. Occlusal-based planning for dental rehabilitation following segmental resection of the mandible and maxilla. ANZ Journal of Surgery 2021;91(3):451-452

11. Mirkhalaf M, Men Y, Wang R, et al. Personalized 3D printed bone scaffolds: a review. Acta Biomaterialia 2022;

12. Al Maruf DSA, Parthasarathi K, Cheng K, et al. Current and future perspectives on biomaterials for segmental mandibular defect repair. International Journal of Polymeric Materials and Polymeric Biomaterials 2022;1-13

13. Al Maruf DS, Ghosh YA, Xin H, et al. Hydrogel: A Potential Material for Bone Tissue Engineering Repairing the Segmental Mandibular Defect. 2022.

14. Zeiter S, Koschitzki K, Alini M, et al. Evaluation of preclinical models for the testing of bone tissue-engineered constructs. Tissue Engineering Part C: Methods 2020;26(2):107-117

15. Manzini BM, Machado LMR, Noritomi PY, et al. Advances in Bone tissue engineering: A fundamental review. Journal of Biosciences 2021;46(1):1-18

16. Urist MR, McLean FC. Osteogenetic potency and new-bone formation by induction in transplants to the anterior chamber of the eye. JBJS 1952;34(2):443-475

17. Yukata K, Xie C, Li T-F, et al. Aging periosteal progenitor cells have reduced regenerative responsiveness to bone injury and to the anabolic actions of PTH 1-34 treatment. Bone 2014;62(79-89

18. Hurrell MJL, Low T-H, Ch'ng S, et al. Fascio-cutaneous and fascio-periosteal free flaps for treatment of intermediate stage osteoradionecrosis of the jaws. Oral Surgery, Oral Medicine, Oral Pathology and Oral Radiology 2022;

19. Albrektsson T, Johansson C. Osteoinduction, osteoconduction and osseointegration. European spine journal 2001;10(2):S96-S101

20. Weber FE. Reconsidering osteoconduction in the era of additive manufacturing. Tissue Engineering Part B: Reviews 2019;25(5):375-386

21. Brånemark R, Brånemark P, Rydevik B, et al. Osseointegration in skeletal reconstruction and rehabilitation. J Rehabil Res Dev 2001;38(2):1-4

Tissue Engineering
Novel sheep model to assess critical-sized bone regeneration with periosteum for in-vivo bioreactors (DOI: 10.1089/ten.TEC.2023.0345)

22. Sartoretto SC, Uzeda MJ, Miguel FB, et al. Sheep as an experimental model for biomaterial implant evaluation. Acta ortopedica brasileira 2016;24(262-266

23. Watson E, Tatara AM, van den Beucken JJ, et al. An ovine model of in vivo bioreactor-based bone generation. Tissue Engineering Part C: Methods 2020;26(7):384-396

24. Mansour M, Wilhite DR, Rowe J. Guide to ruminant anatomy : dissection and clinical aspects. Wiley Blackwell: Hoboken; 2018.

25. Kruse HV, McKenzie DR, Clark JR, et al. Plasma ion implantation of 3D-printed PEEK creates optimal host conditions for bone ongrowth and mineralisation. Plasma Processes and Polymers 2021;18(5):2000219

26. Dindo D, Demartines N, Clavien P-A. Classification of Surgical Complications: A New Proposal With Evaluation in a Cohort of 6336 Patients and Results of a Survey. Annals of Surgery 2004;240(2):205-213

27. Al Maruf DSA, Cheng K, Xin H, et al. A Comparison of In Vivo Bone Tissue Generation Using Calcium Phosphate Bone Substitutes in a Novel 3D Printed Four-Chamber Periosteal Bioreactor. Bioengineering (Basel) 2023;10(10):

28. Chen X, Yu B, Wang Z, et al. Progress of Periosteal Osteogenesis: The Prospect of In Vivo Bioreactor. Orthopaedic Surgery 2022;

29. Tonna EA, Cronkite EP. 23 The Periosteum: Autoradiographic Studies on Cellular Proliferation and Transformation Utilizing Tritiated Thymidine. Clinical Orthopaedics and Related Research (1976-2007) 1963;30(218-236

30. Colnot C, Zhang X, Tate MLK. Current insights on the regenerative potential of the periosteum: molecular, cellular, and endogenous engineering approaches. Journal of Orthopaedic Research 2012;30(12):1869-1878

31. Bettoni J, Olivetto M, Duisit J, et al. Treatment of mandibular osteoradionecrosis by periosteal free flaps. British Journal of Oral and Maxillofacial Surgery 2019;57(6):550-556

32. Xin H, Tomaskovic-Crook E, Al Maruf DSA, et al. From Free Tissue Transfer to Hydrogels: A Brief Review of the Application of the Periosteum in Bone Regeneration. Gels 2023;9(9):768

33. Hewitt L, Yabe T, Wykes J, et al. Defining the dimensions of periosteal free tissue transfer harvest sites. Plastic and Reconstructive Surgery Global Open 2021;9(10):

34. Xin H, Romanazzo S, Tomaskovic-Crook E, et al. Ex Vivo Preservation of Ovine Periosteum Using a Perfusion Bioreactor System. Cells 2023;12(13):1724

35. Brey EM, Cheng M-H, Allori A, et al. Comparison of guided bone formation from periosteum and muscle fascia. Plastic and reconstructive surgery 2007;119(4):1216-1222

TABLE LEGENDS:

Table 1. Complications associated with each experimental animal. Bioreactors in the vascularised wrap design (Group A) were exposed to periosteum only, whereas those in the flat contact design (Group B) were exposed to native bone on the deep surface and periosteum on the superficial surface.

Sheep No	Group	Duration of study (Weeks)	Periosteal Flap	Clavien-Dindo Grade
1	A	0	Wrap	IV
2	A	0	Wrap	IV
3	A	6	Wrap	I
4	A	8	Wrap	Nil
5	A	8	Wrap	Nil
6	A	10	Wrap	Nil
7	A	12	Wrap	Nil
8	A	12	Wrap	Nil
9	B	6	Flat	Nil
10	B	13	Flat	Nil
11	B	14	Flat	I
12	B	14	Flat	I
13	B	14	Flat	Nil
14	B	14	Flat	I

Tissue Engineering
Novel sheep model to assess critical-sized bone regeneration with periosteum for in-vivo bioreactors (DOI: 10.1089/ten.TEC.2023.0345)
This paper has been peer-reviewed and accepted for publication, but has yet to undergo copyediting and proof correction. The final published version may differ from this proof.

Table 2. Different preclinical animal models that incorporate periosteum for assessing bone scaffolds *in vivo*.

Author	Animal	Site
Watson et al 2023 **(35)**	Sheep	Rib Body
Sparks et al 2022 **(1)**	Sheep	Tibia
Tatara et al 2019 **(3)**	Sheep	Rib body
Brey et al 2007 **(34)**	Sheep	Rib body
van Oirschot et al 2022 **(36)**	Pig	Mandible
Runyan et al 2015 **(37)**	Pig	Tibia
Runyan et al 2010 **(38)**	Pig	Rib body
Terheyden et al 1999 **(39)**	Pig	Latissimus dorsi
Puckett et al 1979 **(40)**	Dog	Rib body
Finely et al 1978 **(41)**	Dog	Rib body
Nau et al 2017 **(42)**	Rat	Medial femoral condyle
Pan et al 2018 **(43)**	Rabbit	Tibial flap + femoral defect

Tissue Engineering
Novel sheep model to assess critical-sized bone regeneration with periosteum for in-vivo bioreactors (DOI: 10.1089/ten.TEC.2023.0345)

FIGURE LEGENDS:

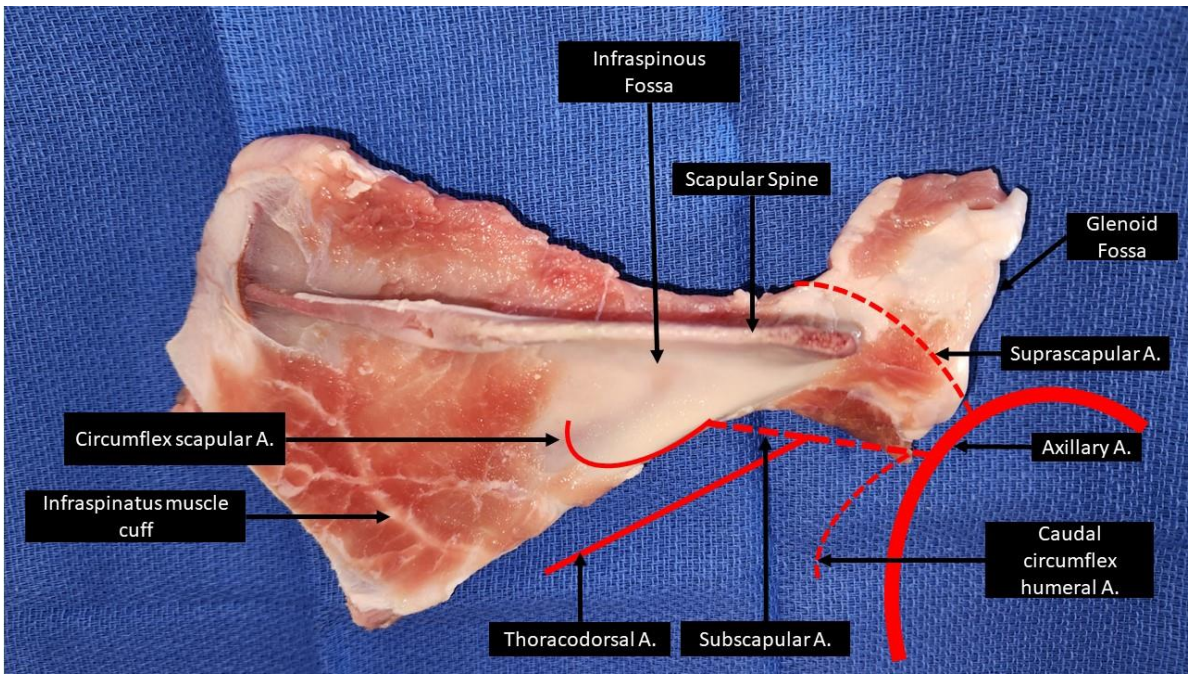

Figure 1. Lateral view of a right sheep scapula labelled with bony landmarks and arterial blood supply superimposed (*red*).

Tissue Engineering
Novel sheep model to assess critical-sized bone regeneration with periosteum for in-vivo bioreactors (DOI: 10.1089/ten.TEC.2023.0345)

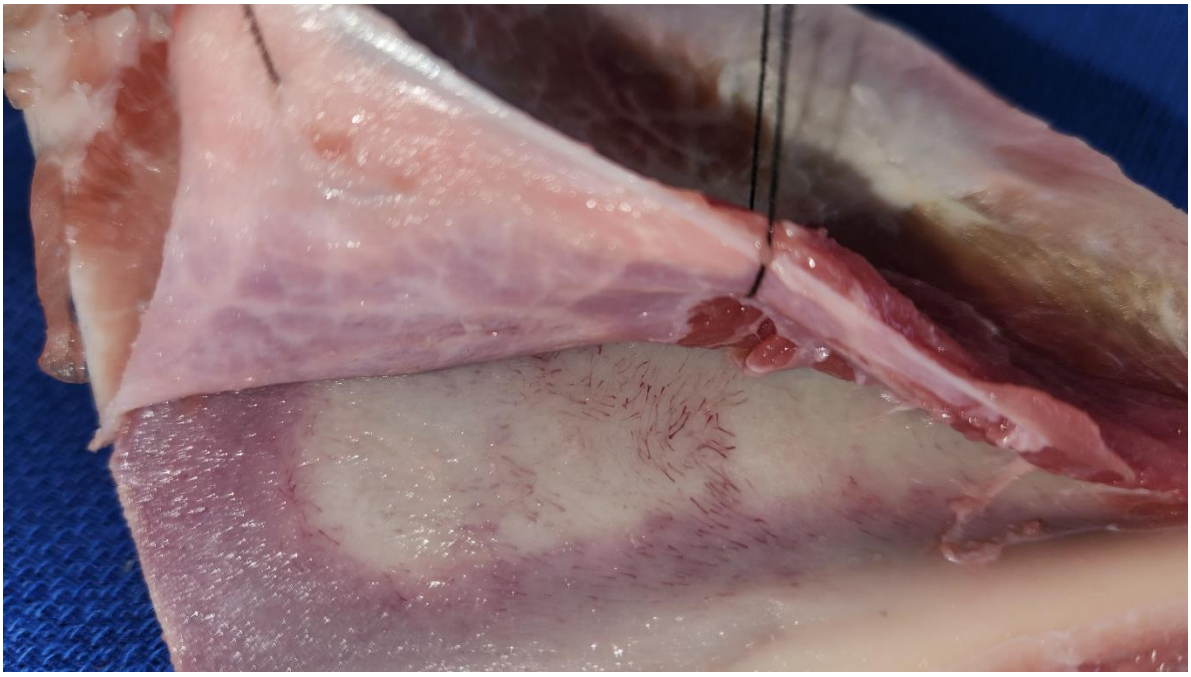

Figure 2. Sheep scapula dissection with the periosteum reflected with attached infraspinatus muscle from the underlying bone. Note that the periosteum fragments closer to the glenoid fossa (right side of figure).

Tissue Engineering
Novel sheep model to assess critical-sized bone regeneration with periosteum for in-vivo bioreactors (DOI: 10.1089/ten.TEC.2023.0345)

Tissue Engineering
Novel sheep model to assess critical-sized bone regeneration with periosteum for in-vivo bioreactors (DOI: 10.1089/ten.TEC.2023.0345)

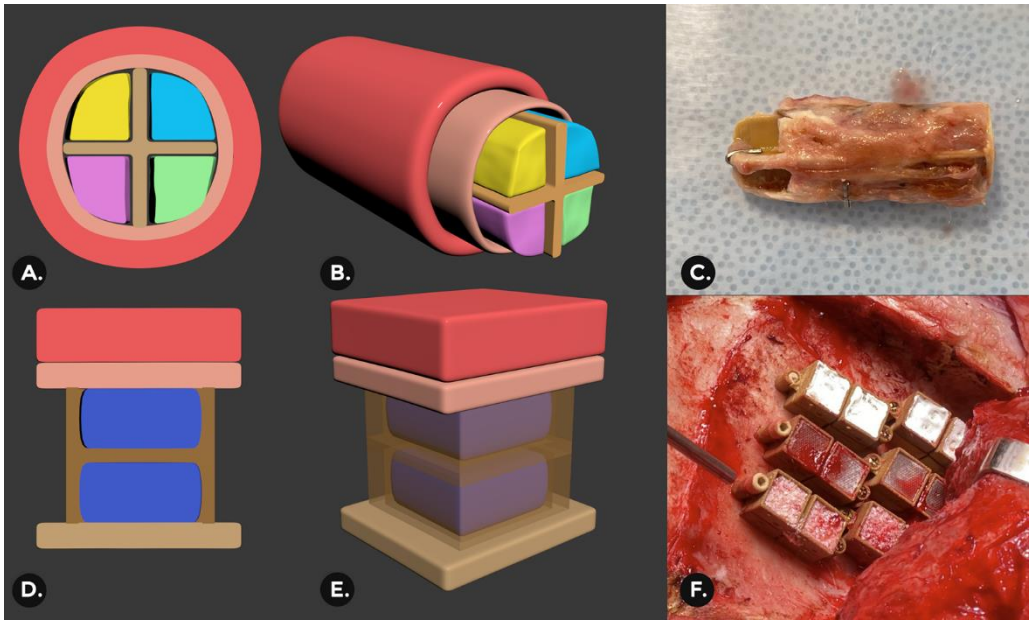

Figure 3. Two bioreactor designs were used in the Ovine models. **A.** Schematic for Group A cross-shaped printed PEEK bioreactors (*dark brown*) were wrapped circumferentially in periosteum (*coral pink*) attached to muscle (*red*). Four different types of biomaterial bone substitutes were tested simultaneously within the bioreactors (*blue*, *green*, *purple,* and *yellow*) **B.** 3D representation of the wrapped PEEK bioreactor. **C.** Explanted PEEK bioreactor with periosteum still intact. **D.** Schematic for Group B, H-shaped printed PEK bioreactor (*dark brown*) allowing for dual contact with bone (light brown) below and periosteum (*coral pink*) above attached to muscle (*red*). The upper and lower chambers were filled with various biomaterials (*dark blue*). **E.** 3D representation of the H-shaped PEK bioreactor. **F.** H-shaped bioreactors implanted with bone below and periosteal flap above.

Tissue Engineering
Novel sheep model to assess critical-sized bone regeneration with periosteum for in-vivo bioreactors (DOI: 10.1089/ten.TEC.2023.0345)

Tissue Engineering
Novel sheep model to assess critical-sized bone regeneration with periosteum for in-vivo bioreactors (DOI: 10.1089/ten.TEC.2023.0345)

Tissue Engineering
Novel sheep model to assess critical-sized bone regeneration with periosteum for in-vivo bioreactors (DOI: 10.1089/ten.TEC.2023.0345)

Tissue Engineering
Novel sheep model to assess critical-sized bone regeneration with periosteum for in-vivo bioreactors (DOI: 10.1089/ten.TEC.2023.0345)
This paper has been peer-reviewed and accepted for publication, but has yet to undergo copyediting and proof correction. The final published version may differ from this proof.

35

Tissue Engineering
Novel sheep model to assess critical-sized bone regeneration with periosteum for in-vivo bioreactors (DOI: 10.1089/ten.TEC.2023.0345)

Tissue Engineering
Novel sheep model to assess critical-sized bone regeneration with periosteum for in-vivo bioreactors (DOI: 10.1089/ten.TEC.2023.0345)

37

Tissue Engineering
Novel sheep model to assess critical-sized bone regeneration with periosteum for in-vivo bioreactors (DOI: 10.1089/ten.TEC.2023.0345)

Tissue Engineering
Novel sheep model to assess critical-sized bone regeneration with periosteum for in-vivo bioreactors (DOI: 10.1089/ten.TEC.2023.0345)

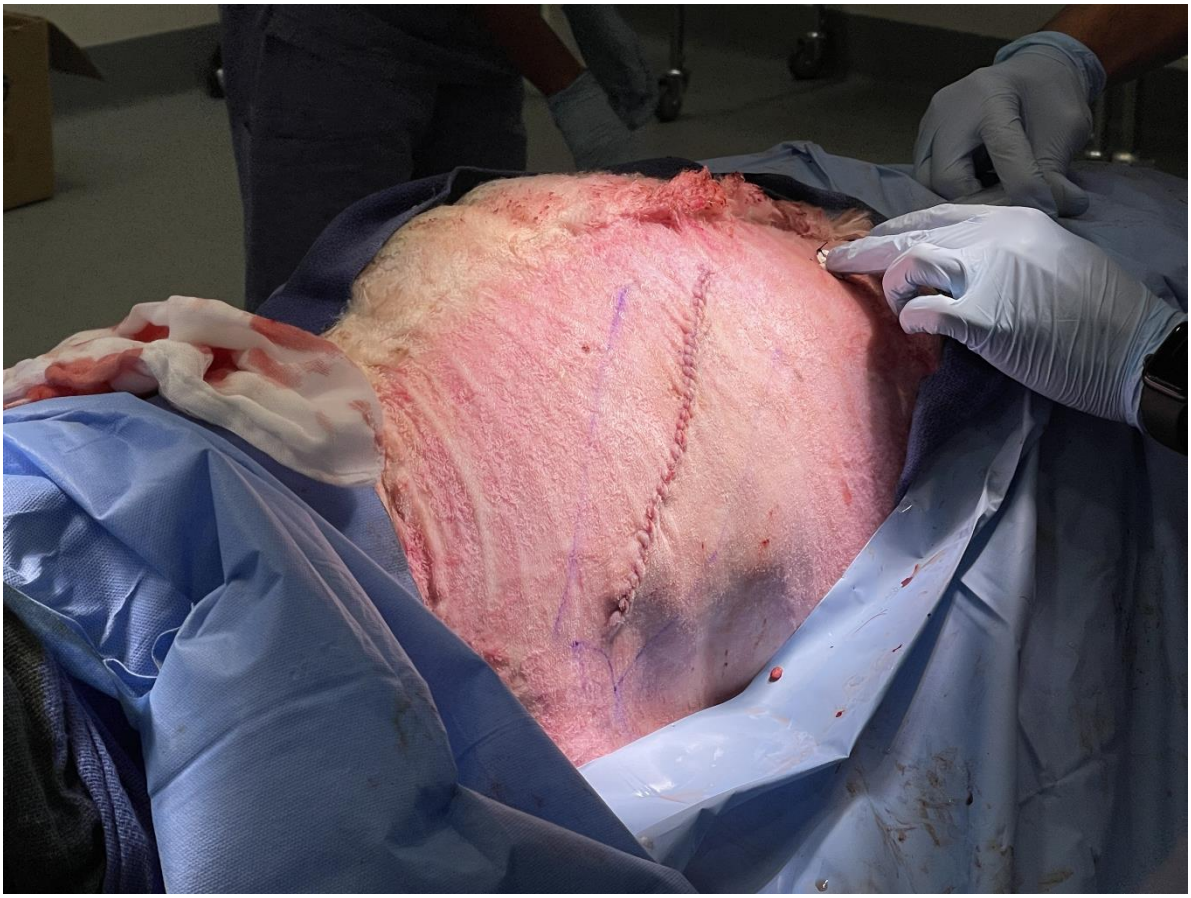

Figure 4. Surgical steps for implanting the Group A scapular periosteal wrap flap in sheep. **A.** Animal draped and scapula landmarks marked. **B.** Sharp dissection onto cutaneous omobrachialis muscles (*arrow*) **C.** Infraspinatus reflected cranially and ventrally (*arrow*) leaving a muscular cuff attached to the underlying periosteum **D.** Thoracic belly of trapezius muscles reflected dorsally (*green arrow*), and periosteum stripped from infraspinous fossa (*yellow arrow*). **E.** Periosteum wrapped around the scaffold (*arrow*). **F.** Periosteal flap in-situ. **G.** Biomaterial packed using an open-ended syringe (*arrow*) **H.** Closed skin wound.

Tissue Engineering
Novel sheep model to assess critical-sized bone regeneration with periosteum for in-vivo bioreactors (DOI: 10.1089/ten.TEC.2023.0345)

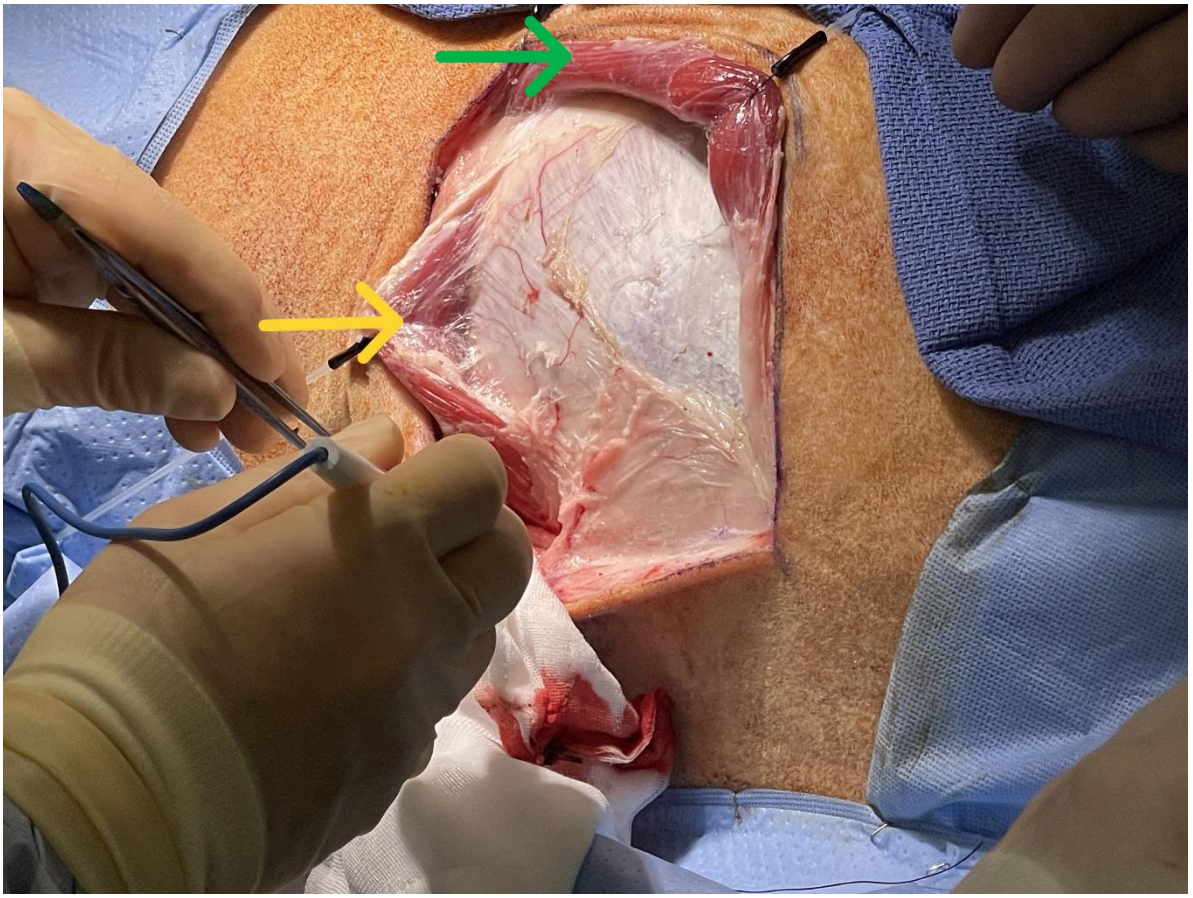

Tissue Engineering
Novel sheep model to assess critical-sized bone regeneration with periosteum for in-vivo bioreactors (DOI: 10.1089/ten.TEC.2023.0345)

Tissue Engineering
Novel sheep model to assess critical-sized bone regeneration with periosteum for in-vivo bioreactors (DOI: 10.1089/ten.TEC.2023.0345)

Tissue Engineering
Novel sheep model to assess critical-sized bone regeneration with periosteum for in-vivo bioreactors (DOI: 10.1089/ten.TEC.2023.0345)
This paper has been peer-reviewed and accepted for publication, but has yet to undergo copyediting and proof correction. The final published version may differ from this proof.

43

Tissue Engineering
Novel sheep model to assess critical-sized bone regeneration with periosteum for in-vivo bioreactors (DOI: 10.1089/ten.TEC.2023.0345)

Tissue Engineering
Novel sheep model to assess critical-sized bone regeneration with periosteum for in-vivo bioreactors (DOI: 10.1089/ten.TEC.2023.0345)
This paper has been peer-reviewed and accepted for publication, but has yet to undergo copyediting and proof correction. The final published version may differ from this proof.

45

Tissue Engineering
Novel sheep model to assess critical-sized bone regeneration with periosteum for in-vivo bioreactors (DOI: 10.1089/ten.TEC.2023.0345)

Figure 5. Surgical steps for implanting the Group B scapular periosteal dual-contact bioreactor in sheep. **A.** Sharp dissection onto cutaneous omobrachialis muscles. **B.** Trapezius (*green arrow*) and latissimus dorsi (*yellow arrow*) muscles separated and reflected away from infraspinatus **C.** Infraspinatus reflected with periosteum **D.** Infraspinous fossa (*arrow*) after complete elevation of musculoperiosteal flap. **E.** Bioreactors (*arrow*) secured to fossa using titanium screws. **F.** Infraspinatus periosteal flap (*arrow*) placed overlying the upper chambers of the bioreactor. **G.** Layered closure incorporating a wound-soaker catheter **H.** Closed skin wound.

Tissue Engineering
Novel sheep model to assess critical-sized bone regeneration with periosteum for in-vivo bioreactors (DOI: 10.1089/ten.TEC.2023.0345)

Tissue Engineering
Novel sheep model to assess critical-sized bone regeneration with periosteum for in-vivo bioreactors (DOI: 10.1089/ten.TEC.2023.0345)

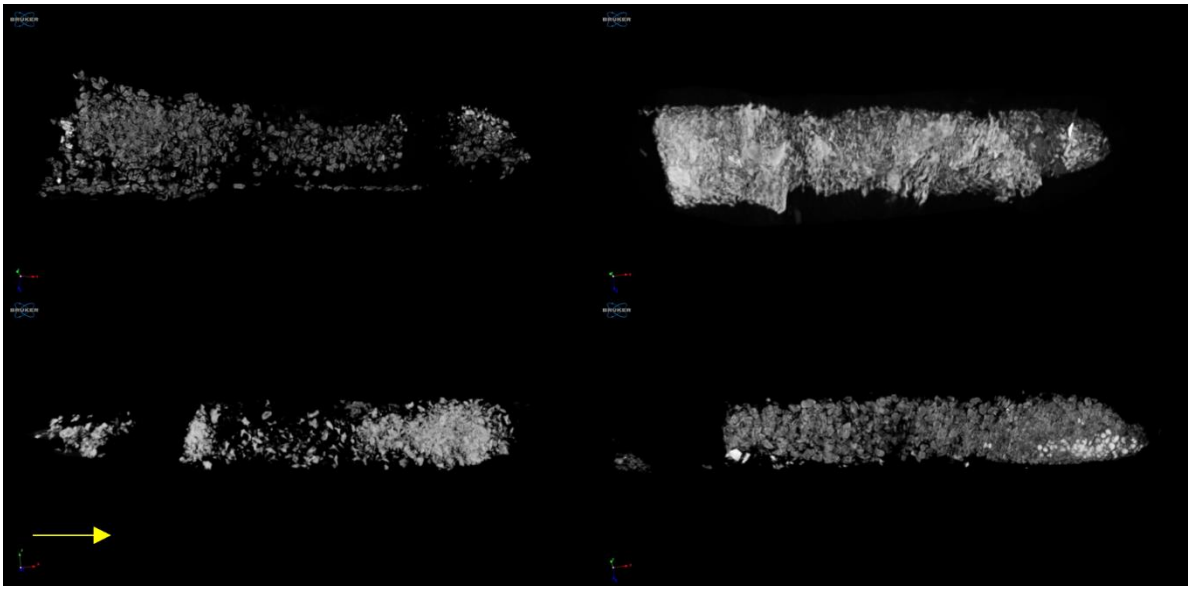

Figure 6. Representative results from 10-week timepoint for Group A periosteal wrap bioreactors **A.** Histological section of the bioreactor with autologous bone (*arrow*), Novabone, BioOss and Zengro chambers (clockwise direction). Bone formation is seen in the autologous chamber, x12.5 **B.** MicroCT of the bioreactor with autologous (*arrow*), Novabone, BioOss and Zengro chambers (clockwise direction).

Tissue Engineering
Novel sheep model to assess critical-sized bone regeneration with periosteum for in-vivo bioreactors (DOI: 10.1089/ten.TEC.2023.0345)

50

Tissue Engineering
Novel sheep model to assess critical-sized bone regeneration with periosteum for in-vivo bioreactors (DOI: 10.1089/ten.TEC.2023.0345)

Tissue Engineering

Novel sheep model to assess critical-sized bone regeneration with periosteum for in-vivo bioreactors (DOI: 10.1089/ten.TEC.2023.0345)

This paper has been peer-reviewed and accepted for publication, but has yet to undergo copyediting and proof correction. The final published version may differ from this proof.

52

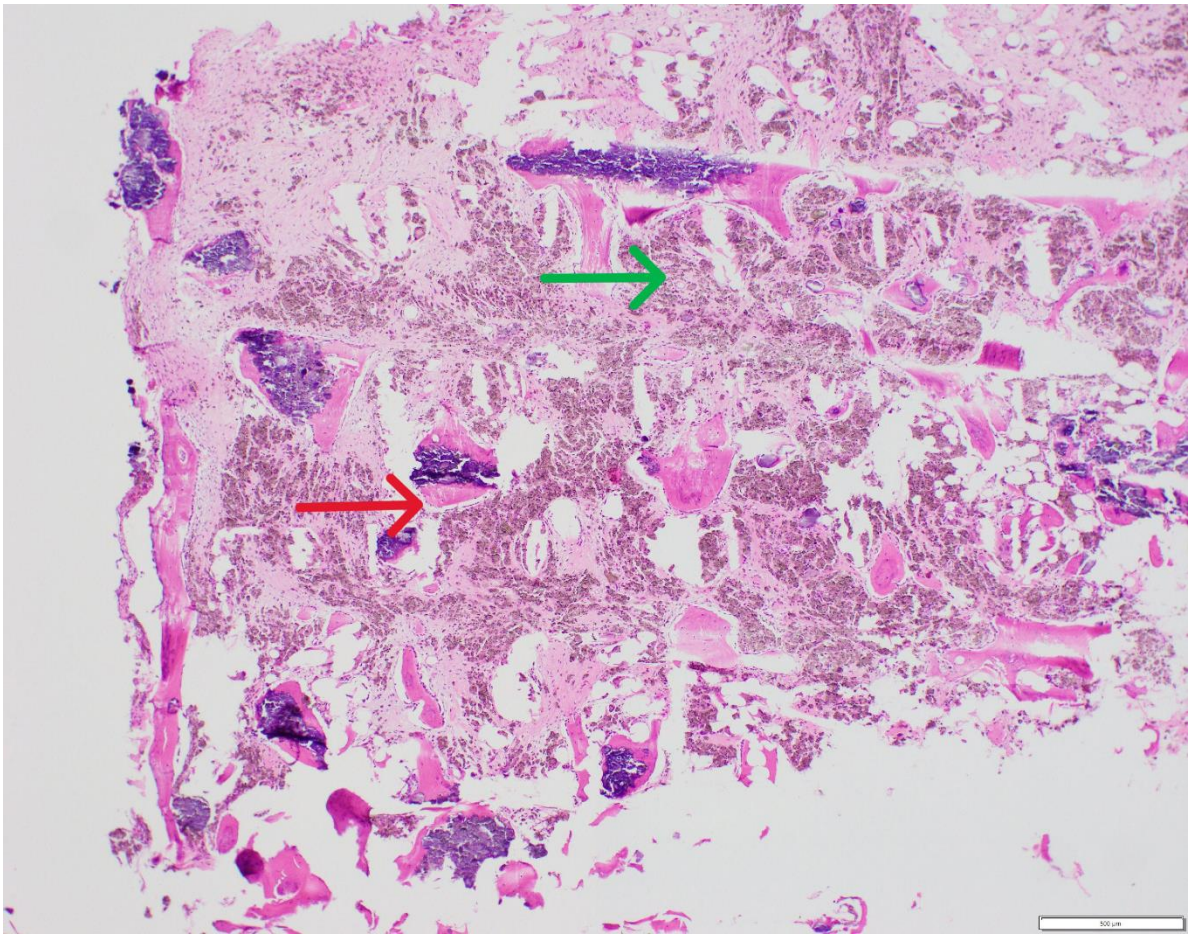

Tissue Engineering
Novel sheep model to assess critical-sized bone regeneration with periosteum for in-vivo bioreactors (DOI: 10.1089/ten.TEC.2023.0345)

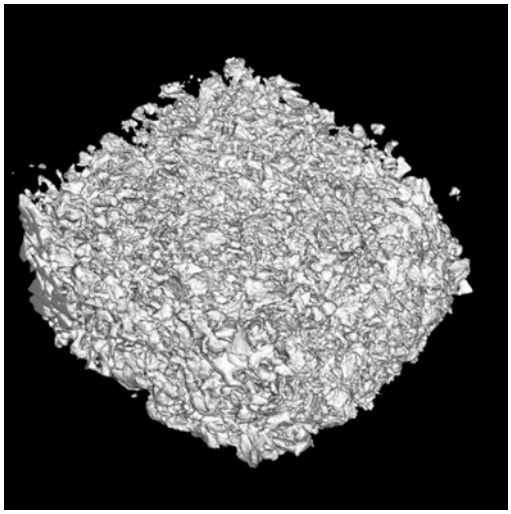

Tissue Engineering
Novel sheep model to assess critical-sized bone regeneration with periosteum for in-vivo bioreactors (DOI: 10.1089/ten.TEC.2023.0345)

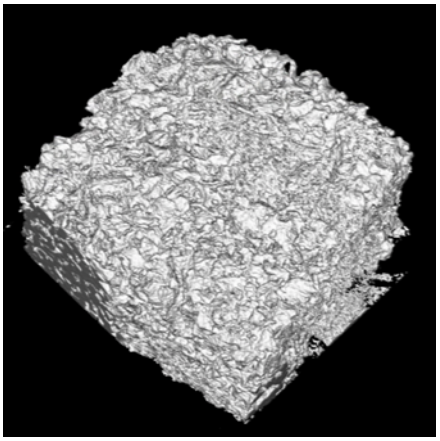

Figure 7. Representative results for Group B dual-contact bioreactors **A.** Upper chamber PCL-GelMA bioreactor with native skeletal muscle (*blue arrow*) and periosteum (*yellow arrow*) above. There is fibrous tissue (*green arrow*) formation in the chamber surrounding the implanted material (*orange arrow*) including some focal lymphocytic inflammatory infiltrate (*red arrow*), x20. **B.** Lower chamber PCL-GelMA reactor with skeletal muscle (*blue arrow*) and native bone (*green arrow*) at the base, implanted material (*yellow arrow*). Focal osteoid production is present at the edge of the chamber (*red arrow*), x20. **C.** Chamber with embedded PCL-GelMA-TCP material showing florid background histiocytic reaction (*green arrow*), but also focal osteoid formation (*red arrow*) surrounding the dense purple implant material, x40. **D.** MicroCT of the Bio-Oss upper chamber in contact with periosteum. **E.** MicroCT of the Bio-Oss lower chamber in contact with native bone.